The biosynthesis of palladium nanoparticles by antioxidants in *Gardenia jasminoides Ellis*: long lifetime nanocatalysts for *p*-nitrotoluene hydrogenation

2009 Nanotechnology 20 385601

(http://iopscience.iop.org/0957-4484/20/38/385601)

Nanotechnology **20** (2009) 385601 (10pp) doi:10.1088/0957-4484/20/38/385601

The biosynthesis of palladium nanoparticles by antioxidants in *Gardenia jasminoides Ellis*: long lifetime nanocatalysts for *p*-nitrotoluene hydrogenation

Lishan Jia[1], **Qian Zhang, Qingbiao Li and Hao Song**

Department of Chemical and Biochemical Engineering, College of Chemistry and Chemical Engineering, Xiamen University, Xiamen 361005, People's Republic of China,
Key Laboratory for Chemistry and Biochemical Engineering, Department of Chemical and Biochemical Engineering, College of Chemistry and Chemical Engineering, Xiamen University, Xiamen 361005, People's Republic of China
and
Key Laboratory for Chemical Biology of Fujian Province, Xiamen University, Xiamen 361005, People's Republic of China

E-mail: jials@xmu.edu.cn

Received 27 May 2009, in final form 27 July 2009
Published 28 August 2009
Online at stacks.iop.org/Nano/20/385601

Abstract

Gardenia jasminoides Ellis' water crude extract was used for the bioreduction of palladium chloride in this paper. The UV–vis spectrum, x-ray diffraction spectrum measurement, the Fourier transform infrared spectroscopy and TEM technique confirmed the formation of palladium nanoparticles and identified antioxidants including geniposide, chlorogenic acid, crocins and crocetin were reducing and stabilizing agents for synthesizing palladium nanoparticles in water crude extract. The particle size and dispersity were temperature-dependent. The particle sizes ranged from 3 to 5 nm and revealed the best dispersity at 70 °C. Catalytic performance of the biosynthetic Pd nanoparticles with good dispersity was investigated by hydrogenation of *p*-nitrotoluene. The catalysts showed a conversion of 100% under conditions of 5 MPa, 150 °C for 2 h. The selectivity of *p*-methyl-cyclohexylamine achieved 26.3%. The catalyst was recycled five times with no agglomeration and maintained activity, which was attributed to the appropriate protection of the antioxidants. On the basis of the study, it appears to be a new promising biosynthetic nanocatalyst for the development of an industrial process.

1. Introduction

The devices and structures ranging from 1 to 100 nm or less have offered unusual optical, chemical, photoelectrochemical and electronic properties different from bulk structures [1, 2]. Nanomaterials such as noble metal materials are at the leading edge of the rapidly developing field of nanotechnology. As catalysts, the metal nanoparticles performed high reactivity and selectivity in various kinds of reactions, such as hydrogenation or dehydrogenation. Kou *et al* obtained Rh nanoparticles in ionic liquid by hydrogen reduction, while the soluble catalyst showed high lifetime and activity in benzene hydrogenation [3]. In recent research, they used Pd nanoparticles solutions for conversion of limonene into *p*-cymene [4].

The sizes, crystal structures, controlled monodispersity and stabilization are the critical factors for the catalytic

[1] Author to whom any correspondence should be addressed.

reactivity of noble metal nanoparticles. The growing interest in the area has led to considerable concern about noble metal nanoparticles' synthetic methods. Chemical reduction in aqueous solutions or non-aqueous solutions [5, 6], microemulsion method [7], template method [8], ultrasonic-assisted method [9] and microwave-assisted synthesis [10] are traditional methods. The control over the particles can be routinely achieved by the above methods [11–14]. However, the nanoparticles' coalescence resulting from aggregation would make them normal, without novel properties. For preventing aggregation, protective agents such as polymers, surfactants and ligands are commonly used [5, 6, 10, 11]. Most of the protective agents and reductants are toxic chemicals which are harmful to the environment. Moreover, the protectivity of particles may not be proper or controllable for further industrial applications.

In addition to conventional chemical and physical methods, biosynthesis of nanoparticles, as a novel method, has gained much attention because of its 'eco-friendly' process and the effective, inexpensive and easily available materials [15, 16]. It is reported that many microorganisms, both unicellular and multicellular, alive or dead are known to produce inorganic nanoparticles both intracellular or extracellular [17–19]. Vigneshwaran *et al* accumulated reasonably monodisperse silver nanoparticles on the surface of *Aspergillus flavus*' cell wall with silver nitrate aqueous solution [19]. Yong *et al* showed that Pd^{2+} could be reduced to Pd^0 by *Desulfovibrio desulfuricans* on the cell surface whether the cell was alive or dead [20]. Biomacromolecules can control the nucleation and their growth of structures. The plant or its extract as a simple and viable reductant also received attention. Gardea-Torresdey *et al* prepared gold nanoparticles by living alfalfa plants [21]. Huang *et al* synthesized different sizes and shapes of silver and gold nanoparticles which could be controlled by varying the amount of *C. camphora* leaf [22]. Shankar *et al* studied bioreduction of chloroaurate ions by geranium leaves and found that its extract and endophytic fungus could yield gold nanoparticles [23]. Further, they tried to control the shape and size of gold nanoparticles by regulating the experimental conditions, such as the amount of lemon grass leaf extract and finally synthesized gold nanotriangles [24]. The biomass used for bioreduction played two roles, respectively, reductant and protective agent.

Nevertheless, biosynthesis is still perplexing owing to the complexity and unknown components in the microorganism or plant. Compared with chemical and physical methods, the particle size is larger and a narrow size distribution is also difficult to achieve. The particles were wrapped round the biomacromolecule which would overprotect them and reduce reactivity in catalytic reactions. Herein, *Gardenia jasminoides Ellis* will be treated with palladium chloride. The plant, known as a herbal medicine for disease treatment and a natural dye for coloring in China, has never been used before for bioreduction. In this study, we try to obtain a new stable tiny grain with narrow size distribution and good dispersity by bioreduction as traditional methods do, avoiding an inappropriate protective effect and performing significant catalytic applications. The catalytic activity of the biosynthetic nanoparticles was investigated in *p*-nitrotoluene hydrogenation. The recycling use of the catalyst was also of concern. The gardenia fruit is easily obtained. The redox experiment was carried out without chemical additives and poisonous by-products under mild reaction conditions. Actually, the fruit's water crude extract is the reductant and stabilizing agent. The mechanism of bioreduction was discussed. The experiments proceeded at different temperatures to investigate the control of the size and shape of the palladium nanoparticles.

2. Materials and methods

2.1. Preparation of water crude extract

The fresh gardenia fruits were harvested from Fujian Province in China. They were put into a drying oven until water removal was complete. The dried fruits were ground into fragments. Then 2 g were boiled with 100 ml deionized water for 5–10 min. After cooling and filtration, the residue was discarded, and the water crude extract of 0.02 g ml^{-1} was used for the reduction of the $PdCl_2$ aqueous solution.

2.2. Synthesis of palladium nanoparticles

The chemical $PdCl_2$ was purchased from Sinopharm Chemical Reagent Co. Ltd, China. 0.025 M $PdCl_2$ aqueous solutions were prepared first. 1 mM $PdCl_2$ reaction mixture was prepared in several Erlenmeyer flasks by adding 1 ml 0.025 M $PdCl_2$ aqueous solution to 24 ml 0.02 g ml^{-1} water crude extract. The flasks were put into a water bath heated for 24 h at different constant temperatures. The reaction temperature was set at equal intervals of 10 °C from 40 to 90 (40, 50, 60, 70, 80 and 90) °C.

2.3. UV–vis spectra test

The bioreduction of palladium ions in water crude extract was monitored by UV–vis spectra of the resulting diluents. Samples of the suspension were diluted with deionized water and subsequently detected. The reaction temperature was 60 °C. UV–vis spectroscopy detection of the water crude extract was carried out as a function of bioreduction time on UNICAM UV-310 (Thermo Spectronic) spectrophotometers at a resolution of 1 nm. The spectra were recorded in the region of 190–500 nm.

2.4. XRD measurement

The water crude extract and the reaction liquid after bioreduction were dried at 45 °C in a vacuum drying oven. Then the dried mixture was collected for the determination of the formation of palladium nanoparticles. The measurement was taken at a voltage of 40 kV and a current of 30 mA with Cu Kα radiation by an X'Pert Pro x-ray diffractometer (PANalytical BV, The Netherlands). The pattern was recorded in the region of 30°–90°.

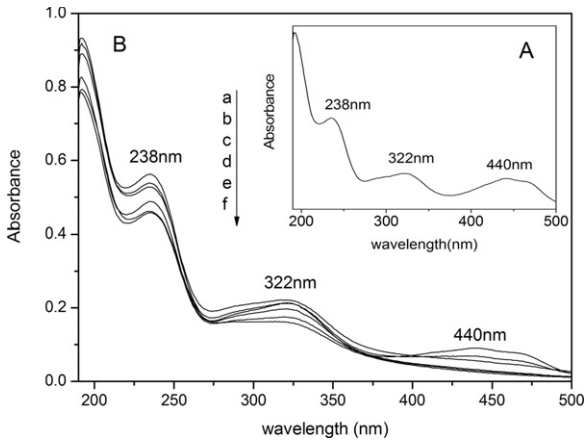

Figure 1. Absorption spectrum of water crude extract with palladium chloride at 60 °C ($C_{Pd^{2+}}$ = 1 mM; a: 5 min; b: 10 min; c: 1.5 h; d: 5 h; e: 12 h; f: 24 h; (A) absorption spectrum of water crude extract).

2.5. FTIR analysis

The reaction liquid and the water crude extract were dried at 45 °C in a vacuum drying oven. The biomass before bioreduction and the residue of water crude extract after bioreduction were analyzed by FTIR Nicolet Avatar 660 (Nicolet, USA). The samples were prepared by mixing the residue with KBr at a ratio of 1:100. The spectra were recorded in the region of 4000–400 cm^{-1}.

2.6. TEM observation of palladium nanoparticles

TEM samples of the aqueous suspension of palladium nanoparticles were prepared by placing a drop of the suspension on carbon-coated copper grids and allowing the water to evaporate. After catalytic reaction, the particle catalysts were filtered, washed with ethanol and dispersed in ethanol by ultrasonication. Then the ethanol suspension was dropped onto the carbon-coated copper grids and the ethanol was allowed to evaporate. HRTEM and TEM observations were performed on a JEM-2100 electron microscope operated at an accelerating voltage of 200 kV. The energy-dispersive x-ray (EDX) analyses and electron diffraction (ED) measurements were performed too. The size distribution of the nanoparticles was estimated on the basis of TEM micrographs with the assistance of SigmaScan Pro software (SPSS Inc., version 4.01.003).

2.7. p-nitrotoluene hydrogenation

The catalytic reactions were carried out in a 0.3 L magnetically stirred high pressure reactor. 0.04 g Pd catalyst (0.25 g biomass contained 2.6 mg Pd), 3.5 g *p*-nitrotoluene and 25 ml isopropanol were added to the 0.3 L reactor at 150 °C under constant hydrogen pressure (5 MPa) for 2 h. After reaction, the catalyst was recovered by vacuum drawing and filtering for recycling use, and the product was collected. The conversion and selectivity were calculated by gas chromatography (GC-950).

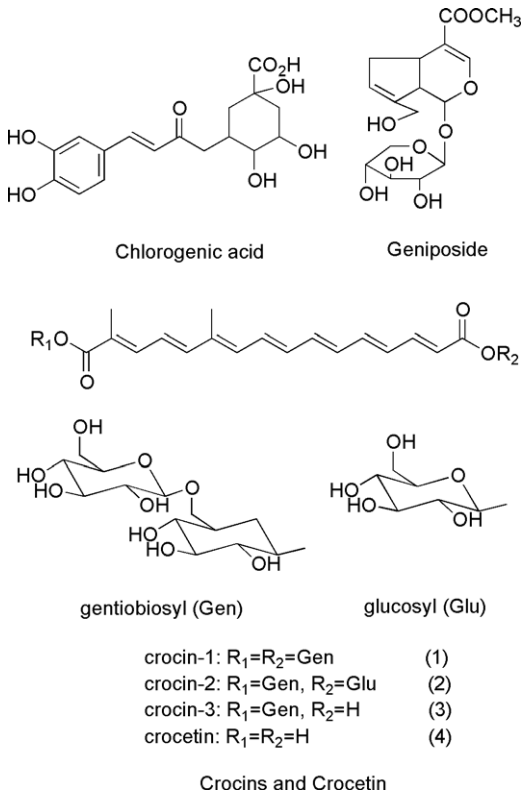

Figure 2. Structures of geniposide, chlorogenic acid, crocins and crocetin.

3. Results and discussion

3.1. UV–vis spectra analysis

After mixing the solution of palladium chloride with water crude extract, the water crude extract changed gradually from transparent orange to dark brown. The new color was ascribed to the excitation of surface plasmon vibrations in the palladium nanoparticles, which indicated the formation of Pd^0 directly. Figure 1 shows the absorption spectra with time intervals of water crude extract reacting with palladium chloride at 60 °C. The peak assigned to Pd^{2+} was not found, and just the evolution of gardenia jasminoides' water crude extract was presented. The curve of palladium ions might be covered up by the water crude extract's which showed a more powerful absorption strength. The absorption peaks at 238 nm and 322 nm are, respectively, the characteristic peaks of geniposide [25] and chlorogenic acid [26], and the peak at 440 nm is assigned to crocins and crocetin [27]. Geniposide, chlorogenic acid, crocins and crocetin are the main components of the water crude extract, and are all antioxidants [27–29]. Figure 2 shows their structures. Carbonyl, carboxyl, and especially abundant hydroxyl, were determined in their structures. After 1.5 h of the reaction, the peak at 440 nm disappeared (curve c in figure 1(B)) and other characteristic peak absorbances were reduced with increasing reaction time. Since 12 h (curve e in figure 1(B)), the curve absorbance did not reduce anymore. It showed the interaction between palladium chloride and the organic compounds would be finished in 24 h at this temperature.

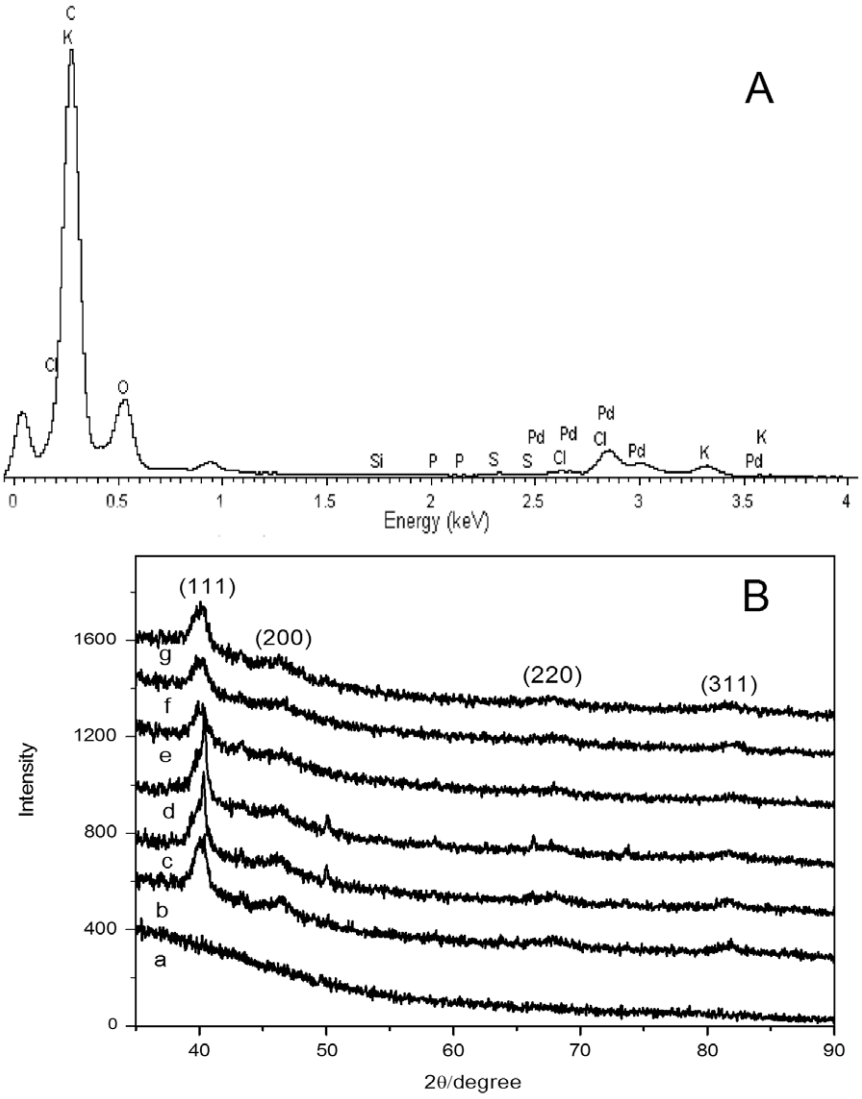

Figure 3. Energy-dispersive x-ray spectrum (A) and x-ray diffraction patterns (B) of palladium nanoparticles generated at 60 °C ($C_{Pd^{2+}} = 1$ mM; a: dried powder of water crude extract; b: 5 h; c: 8 h; d: 12 h; e: 16 h; f: 20 h; g: 24 h).

3.2. Energy-dispersive x-ray (EDX) and x-ray diffraction (XRD) characterization

Energy-dispersive x-ray analysis is shown in figure 3(A). The Pd element signal is indicated. Other elements, such as C, O, K and S, are from the materials in the water crude extract. X-ray diffraction (XRD) confirmed the generation of Pd^0 (figure 3(B)).

XRD measurements can describe an accurate analysis for the formation of new compounds and phases. The phase composition and crystal can be borne out by comparing the scanning curve with the diffraction peak in reported data. Figure 3(B) shows XRD patterns of the dried powder crude extract before and after different reduction times. Compared with the diffraction peak of the water crude extract (pattern a in figure 3(B)), the appearance of new diffraction peaks was due to redox. The diffraction peaks at 40°, 46°, 68° and 82° were indexed to the (111), (200), (220) and (311) planes of palladium in the reported database. It suggested Pd^{2+} was reduced to Pd^0 and the particles had a cubic (fcc) structure. The impure peaks may result from the crude extract. In addition, the particle diameter was 3.9 nm, calculated by the Sheryl formula, which was in accord with the results from TEM images and size distribution (figures 5(F) and 7(C)).

3.3. FTIR characterization of significant functional groups

As shown in figure 4, FTIR measurements were carried out to identify the possible functional groups responsible for the reduction and efficient stabilizing of the metal nanoparticles. Curve a in figure 4 represents the FTIR spectrum of the dried power of water crude extract and shows peaks at 1756, 1701, 1384, 1282, 1081 and 1049 cm^{-1}. The peaks at 1756 and 1701 cm^{-1} were associated with C=O stretching vibration in carboxylic acids or unsaturated esters. The peak at 1384 cm^{-1} was assigned to a carboxyl group. The peaks at 1282 and 1049 cm^{-1} were assigned to C–O stretching vibration in phenolic compounds and –C=CCOOR, respectively. The

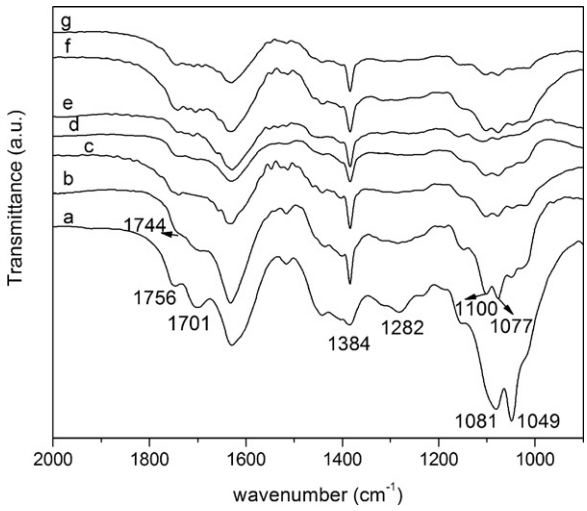

Figure 4. Typical FTIR absorption spectra of dried residue of water crude extract with palladium nanoparticles before and after bioreduction ($C_{Pd^{2+}} = 1$ mM; 24 h; a: dried power of water crude extract; b: 40 °C; c: 50 °C; d: 60 °C; e: 70 °C; f: 80 °C; g: 90 °C).

peak at 1081 cm^{-1} corresponded to the coupled vibrations ($\delta_{O-H} + \nu_{C-O}$) of the hydroxyl group. The overall observation was in line with the organic compounds in figure 2. Curves b–g represent the FTIR spectrum of the water crude extract with palladium chloride solution at different temperatures after bioreduction. The peak at 1756 cm^{-1} had a blueshift to 1744 cm^{-1}. The band at 1701 cm^{-1} was reduced at 40 °C (curve b in figure 4) and disappeared at higher temperatures. Earlier studies on the protection of palladium nanoparticles by poly-(vinylpyrrolidone) (PVP) have proved that the interaction between the particle surface and C=O was the determinant [30, 31]. The evolution of the peaks confirmed the protection of C=O···Pd. The peak at 1384 cm^{-1} appeared stronger after reaction, while the strength of the peaks at 1282 and 1049 cm^{-1} was reduced at 40 °C (curve b) and totally vanished at 50–90 °C. The evolution was attributed to the coordination between C–O and palladium particles. The peak at 1081 cm^{-1} disappeared after bioreduction and two new peaks located at 1077 and 1100 cm^{-1} were detected, which dealt with the reduction of palladium ions by hydroxyl and complexation of Pd^{2+} with the oxygen from hydroxyl. As the reduction proceeded, a new band assigned to C=O should appear at 1600–1800 cm^{-1}. However, the curves did not show any band in this region. It might be overlaid by other higher frequency bands. It is noted that the antioxidants were indeed responsible for the reduction and stabilization of palladium particles and the redox was temperature-dependent. Palladium ions coordinated with the antioxidants by C=O and C–O, and were *in situ* reduced to Pd^0. The stabilization and protection of palladium particles were carried out through C=O···Pd, –C–O···Pd and –CO–O···Pd.

3.4. TEM images of palladium nanoparticles

Representative high-resolution TEM images shown in figure 5 recorded different shapes of palladium nanoparticles which arose from the bioreduction of palladium chloride by water crude extract at each temperature for 24 h. The structures of the particles at 40 °C were diverse. Well-defined morphologies with spherical, rod and three-dimensional polyhedra were observed. Nevertheless, only spherical or near-spherical particles appeared at other reaction temperatures. It is suggested that the variety of particle shapes was favored at lower temperatures. All the palladium nanoparticles presented lattice images in the HRTEM images. The lattice constant calculated from the pattern was 2.3 Å (figure 5(J)), a value in agreement with the spacing between (111) planes. The selected-area electron diffraction pattern (figure 5(K)) supported the fcc crystalline structure of metallic palladium.

Figures 6(A)–(F) showed the TEM films of palladium nanoparticles at different reaction temperatures. The particles showed the best dispersity at 70 °C (figure 6(D)), while the bigger particles agglomerated at 50 °C (figure 6(B)). Palladium nanoparticles generated at 70 °C revealed a high degree of monodispersion without any agglomeration. The palladium nanoparticles adhered on the faint thin layers of other materials which acted as the supporter. The materials were supposed to be the stabilizers in the water crude extract, which was confirmed by the FTIR study above.

The particle size distribution patterns are shown in figure 7. From 40 °C to 90 °C, the average particle size was found to be 13.63 nm, 5.70 nm, 4.47 nm, 4.95 nm, 4.68 nm and 5.14 nm, respectively. They all possessed narrow size distributions. The particle sizes mostly ranged from 3 to 5 nm generated at 60–90 °C, while at 40 °C the scale was 13–15 nm and at 50 °C more tiny particles were present. A minority of tiny palladium crystal nuclei formed in the beginning since the reaction proceeded relatively slowly at 40 and 50 °C. The temperature was inappropriate for forming more crystal nuclei. As seeds, the nuclei subsequently grew up gradually by further reduction of Pd^{2+} and formed a variety of larger particles. Particle assembly played a predominant role in the process. While excited by the increasing temperature from 60 to 90 °C, greater quantities of crystal nuclei were available to form during the first period. The formation of tiny spherical particles competed with the assembly of crystal nuclei. The palladium ions were consumed too rapidly to grow larger. The particles ranging from 3 to 5 nm were almost 80% from 70 to 90 °C. Although no additional protective agents were added, the particle size of 3–5 nm was more or less comparable to those synthesized in the presence of stabilizing agents [11, 30, 32–34]. Consequently, confirmed by the particle size, dispersity and distribution study, 70 °C was the optimum temperature for palladium nanoparticle preparation. The above results indicated that the particles' morphology and dispersity were temperature-controlled, which was consistent with the FTIR analysis.

3.5. The catalytic activity evaluation

The reactivity of Pd catalyst prepared at different temperatures was shown in table 1. *p*-toluidine and *p*-methyl-cyclohexylamine are the only products detected by gas chromatography. The hydrogenation occurred in two steps,

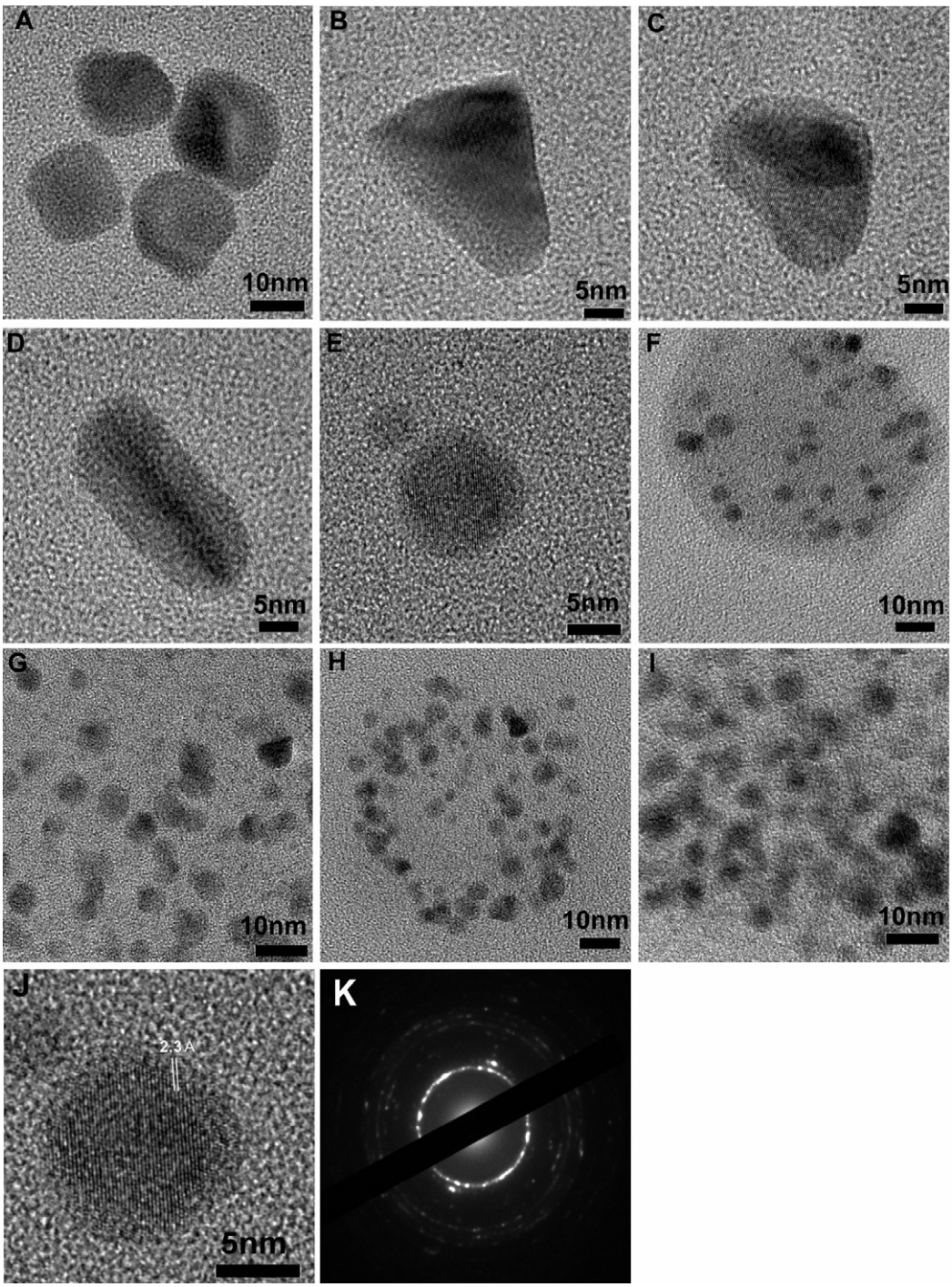

Figure 5. High-resolution transmission electron micrographs of a variety of palladium nanoparticles resulting from each temperature ((A)–(J)) and electron diffraction pattern of palladium nanoparticles raised from 60 °C (K) ($C_{Pd^{2+}} = 1$ mM; 24 h; (A)–(D): 40 °C; (E): 50 °C; (F): 60 °C; (G): 70 °C; (H): 80 °C; (I): 90 °C; (J): 50 °C; (K): 60 °C, 20 μm).

first *p*-nitrotoluene was converted to *p*-toluidine, and then *p*-methyl-cyclohexylamine was generated. In the experiments, the different catalysts were the critical factor among other constant conditions. The conversion and selectivity were catalyst-dependent (table 1). *p*-nitrotoluene was completely converted on the use of catalysts which were biosynthesized at 70 and 80 °C. The yield of *p*-methyl-cyclohexylamine climbed above 20% with the use of the catalysts prepared at 70–90 °C. The minimum yield of *p*-methyl-cyclohexylamine was 8.9% and the maximum yield was 26.3%. It is noted that the activity increased with the bioreduction temperature until 80 °C and was lowered a little at 90 °C. The above results were uniform with the TEM analysis of palladium nanoparticles, which suggested that proper particle diameters, good dispersity and narrow size distribution would certainly lead to high conversion and better selectivity. It meant that the catalysts prepared at 70 and 80 °C were the best choices for the hydrogenation system.

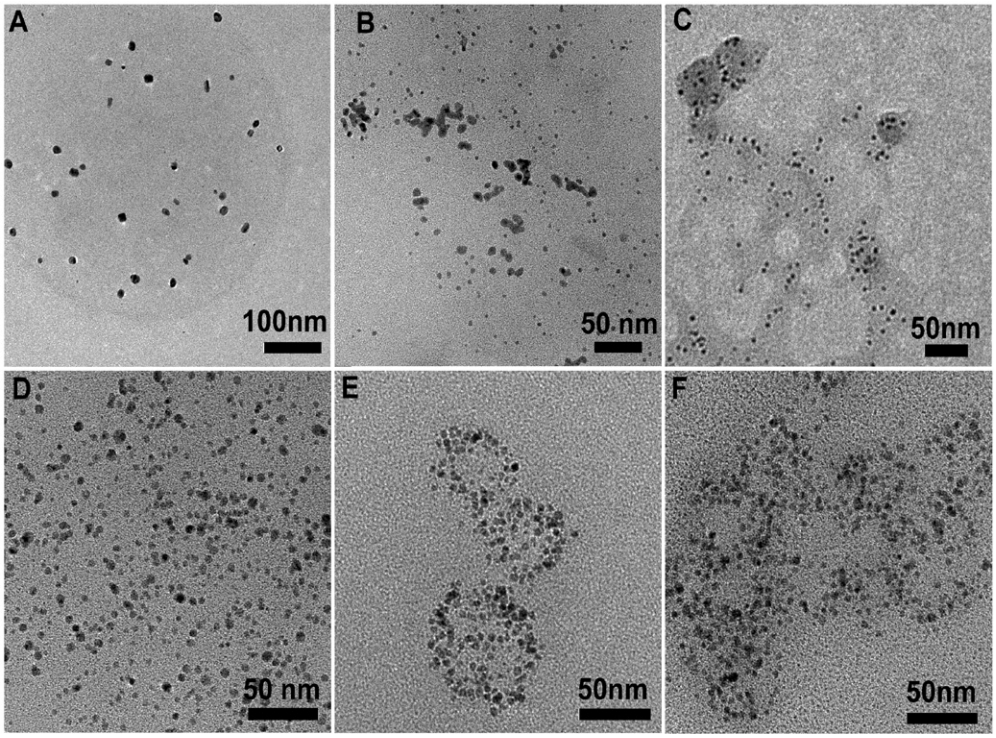

Figure 6. Transmission electron micrographs of palladium nanoparticles after bioreduction ($C_{Pd^{2+}} = 1$ mM; 24 h; (A) 40 °C; (B) 50 °C; (C) 60 °C; (D) 70 °C; (E) 80 °C; (F) 90 °C).

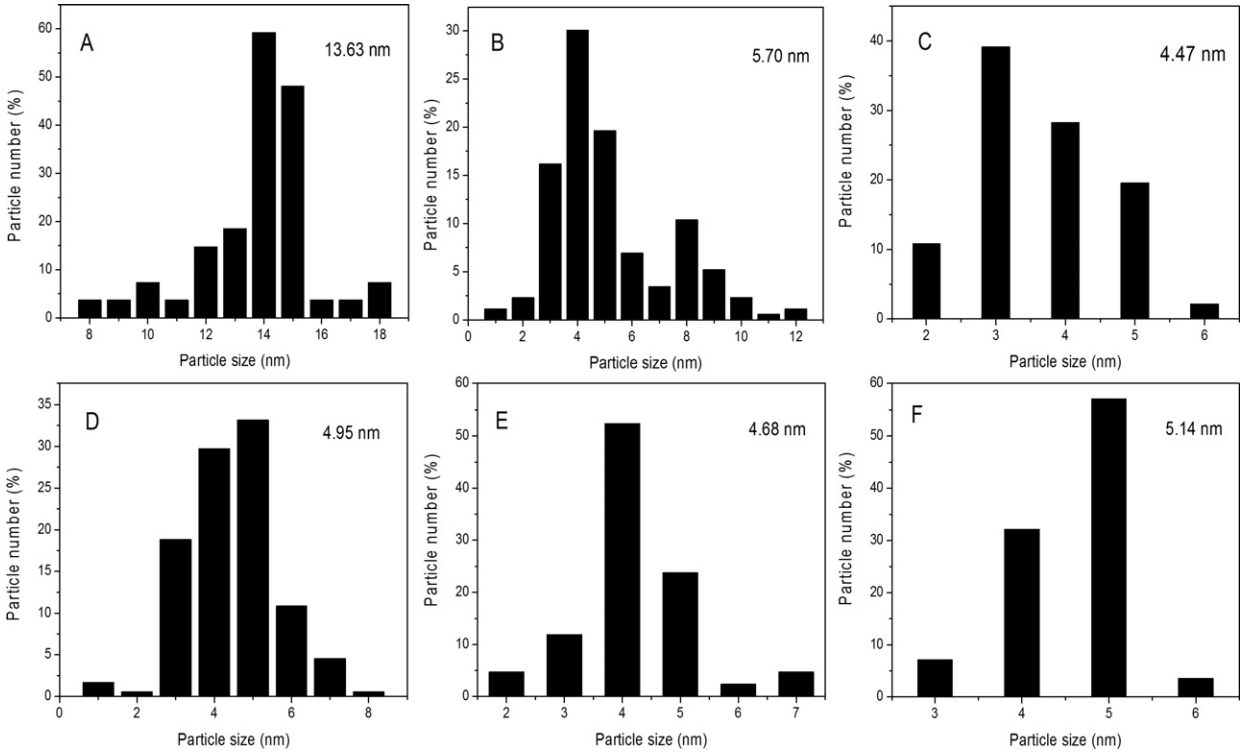

Figure 7. Size distribution of palladium nanoparticles ($C_{Pd^{2+}} = 1$ mM; 24 h; (A) 40 °C; (B) 50 °C; (C) 60 °C; (D) 70 °C; (E) 80 °C; (F) 90 °C).

The TEM film of the catalyst (prepared at 70 °C) after five cycles was shown in figure 8. The freshly prepared and recovered catalyst exhibited a little growth of 4.95 nm (figures 7(D) and 8(B)) to 5.22 nm, which was due to the Ostwald ripening process. Compared with figure 6(D), the catalyst did not show any agglomeration and maintained good dispersity. Table 2 shows the conversion of *p*-nitrotoluene hydrogenation and selectivity of the catalyst obtained at 70 °C

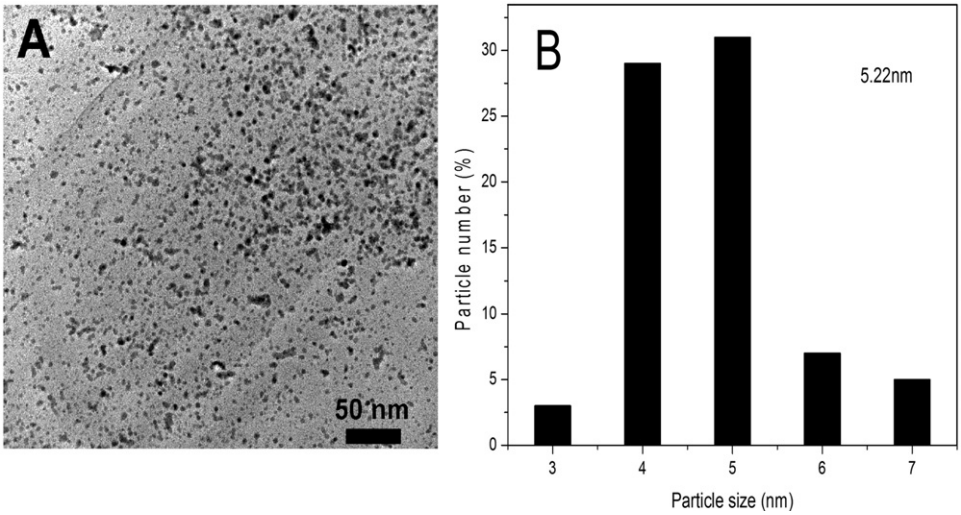

Figure 8. TEM and size distribution of catalyst after hydrogenation (catalyst: prepared at 70 °C; reaction conditions: 150 °C, constant hydrogen pressure of 5 MPa, 2 h).

Table 1. The conversion and selectivity of hydrogenation using different catalysts. (Note: conditions: 0.04 g Pd catalyst (Pd, 0.416 mg), 3.5 g *p*-nitrotoluene, 25 ml isopropanol; 150 °C, 5 MPa H_2, 2 h. The Pd catalysts were prepared at different temperatures.)

		Selectivity[a] (%)	
Catalyst (°C)	Conversion[a] (%)	*p*-toluidine	*p*-methyl-cyclohexylamine
60	98	83.4	16.6
70	100	78.6	21.4
80	100	73.7	26.3
90	95	77.8	22.2

[a] Determined by GC analysis.

Table 2. Recycling of *p*-nitrotoluene hydrogenation using biosynthetic Pd catalyst. (Note: conditions: 0.04 g Pd catalyst (Pd, 0.416 mg), 3.5 g *p*-nitrotoluene, 25 ml isopropanol; 150 °C, 5 MPa H_2, 2 h. The Pd catalyst was obtained at 70 °C.)

		Selectivity[a] (%)	
Cycle number	Conversion[a] (%)	*p*-toluidine	*p*-methyl-cyclohexylamine
1	100	78.6	21.4
2	100	77.3	22.7
3	100	78.2	21.8
4	100	77.5	22.5
5	100	77.8	22.2

[a] Determined by GC analysis.

for five cycles. No loss in activity was found throughout the recycling. All the conversion of the hydrogenation reaction was 100%. It determined a total turnover number (TON) of 37 000 (in five recycle times of 7400 each) and a total turnover frequency (TOF: based on mole *p*-nitrotoluene conversion per total mole metal per hour during the reaction time) of 3700 h^{-1} in 10 h. Based on *p*-methyl-cyclohexylamine, the TOF was 973 h^{-1}. The maintained activity confirmed no further agglomeration occurred, which proved the particles' protection of the antioxidants was stable and appropriate in the catalytic reaction. As the crocins and crocetin are polyhydroxy compounds, combining with the solvent isopropanol, they provided good conditions for rotating of the metal catalysts in the reaction system and made sufficient contact between the catalysts and *p*-nitrotoluene. In addition, they apparently adhered to the metal particles as a faint thin layer (figure 6) which was supposed to be the support in the reaction system. In contrast, with a traditionally supported metal catalyst, the catalyst was not restricted to the support surface but complexed with the novel support, producing more active sites and making it a highly efficient catalyst.

There is no suitable literature on *p*-nitrotoluene hydrogenation; therefore analogous reactions were examined. *p*-nitrotoluene was easily converted into *p*-toluidine by hydrogenation, thus just aromatic hydrogenation was considered and the comparison of metal catalysts for arene hydrogenation was provided in table 3. Ru, Rh and Pt catalysts exhibit excellent activity in benzene and its derivatives of hydrogenation, while Pd was seldom reported. Takasaki *et al* showed that Ru/CNF-P (carbon nanofiber platelet) catalyst was effective for aniline hydrogenation and gave a TOF of 579 h^{-1} (table 3, entry 4) [35]. Under similar conditions, the biosynthetic Pd catalyst gave a TOF (based on mole *p*-methyl-cyclohexylamine generation per total mole metal per hour during the reaction time) of 612 h^{-1} for *p*-nitrotoluene hydrogenation (table 3, entry 2). Rh nanoparticles stabilized by the ionic-liquid-like copolymer poly were used to catalyze the hydrogenation of *p*-xylene in ionic liquids and determined a TOF of 68 h^{-1} for *p*-xylene hydrogenation (table 3, entry 5) [36]. Compared with Ru and Rh catalysts for hydrogenation of other analogous compounds, the biosynthetic Pd catalyst was still superior.

4. Conclusions

In conclusion, a process for the biosynthesis of stable palladium nanoparticles using *Gardenia jasminoides Ellis*' water crude extract was demonstrated. The reducing and

Table 3. The comparison of arene hydrogenation catalyzed by metal catalyst.

Entry	Substrate	Catalyst	Product/TOF[a] (h^{-1})	
1[b]	*p*-nitrotoluene	Pd[c]	*p*-methyl-cyclohexylamine/973	This work
2[d]	*p*-nitrotoluene	Pd[c]	*p*-methyl-cyclohexylamine/612	
3[e]	*p*-nitrotoluene	Pd[c]	*p*-methyl-cyclohexylamine/128	
4[f]	Aniline	Ru	Cyclohexylamine/579	[35]
5[g]	*p*-xylene	Rh	1, 4-dimethyl-cyclohexane/68	[36]

[a] TOF based on mole product per total mole metal per hour during the reaction time.
[b] Conditions: 0.04 g Pd catalyst (Pd, 0.416 mg), 3.5 g *p*-nitrotoluene, 25 ml isopropanol; 150 °C, 5 MPa H_2, 2 h.
[c] The Pd catalyst was obtained at 80 °C.
[d] Conditions: 0.04 g Pd catalyst (Pd, 0.416 mg), 3.5 g *p*-nitrotoluene, 25 ml isopropanol; 100 °C, 3 MPa H_2, 2 h.
[e] Conditions: 0.04 g Pd catalyst (Pd, 0.416 mg), 3.5 g *p*-nitrotoluene, 25 ml isopropanol; 50 °C, 3 MPa H_2, 2 h.
[f] Conditions: Ru/CNF-P (1.7 wt% Ru, 5 mg), 1 ml aniline; 100 °C, 3 MPa H_2, 24 h; TON = 13900; CNF-P: carbon nanofiber platelet.
[g] Conditions: 1.6×10^{-5} mol Rh in 6 ml [BMIM][BF_4], [*p*-xylene]/[Rh] = 2000, ionic-liquid-like copolymer/Rh = 5:1 (mol/mol); 4 MPa H_2, 75 °C, 12 h.

protective agents for synthesizing palladium nanoparticles were identified to be antioxidants in the water crude extract. The particle size, shape and dispersion were preparation temperature-dependent. Hence, the catalyst activity was correlated indirectly with bioreduction temperature. The metal catalyst performed high conversion and reactivity in *p*-nitrotoluene hydrogenation. In this case, the antioxidants played an excellent role of stabilizers without being overprotective. The green synthesis of palladium nanoparticles has original advantages of being environmentally benign and mild reaction conditions as a biological method. Furthermore, a narrow size distribution and diameter have achieved the level of chemical methods. The biosynthetic metal nanocatalyst exhibited excellent activity performance in the hydrogenation system and their stability was manifested in recycling use, endowing them with industrial value.

Acknowledgments

This work is supported by the National Natural Science Foundation of China (grant nos. 20776120 and 20576109) and the National High Technology Research and Development Program of China (863 Program, grant no. 2007AA03Z347). The authors thank the Analysis and Testing Center of Xiamen University for the analysis and observational work in this study.

References

[1] Bhattacharya R and Mukherjee P 2008 *Adv. Drug. Deliv. Rev.* **60** 1289–306
[2] Klefenz H 2004 *Eng. Life Sci.* **3** 211–8
[3] Mu X, Meng J, Li Z and Kou Y 2005 *J. Am. Chem. Soc.* **127** 9694–5
[4] Zhao C, Gan W, Fan X, Cai Z, Dyson P J and Kou Y 2008 *J. Catal.* **254** 244–50
[5] Chaki N K, Sharma J, Mandle A B, Mulla I S, Pasricha R and Vijayamohanan K 2004 *Phys. Chem. Chem. Phys.* **6** 1304–9
[6] Wang X Q, Itoh H, Naka K and Chujo Y 2003 *Langmuir* **19** 6242–6
[7] Maillard M, Giorgio S and Pileni M P 2003 *J. Phys. Chem.* B **107** 2466–70
[8] Faure C, Derre A and Neri W 2003 *J. Phys. Chem.* B **107** 4738–46
[9] Johans C, Clohessy J, Fantini S, Kontturi K and Cunnane J V 2002 *Electrochem. Commun.* **4** 227–30
[10] Komarneni S, Li D S, Newalkar B, Katsuki H and Bhalla A S 2002 *Langmuir* **18** 5959–62
[11] Yonezawa T, Imamura K and Kimizuka N 2001 *Langmuir* **17** 4701–3
[12] Yang Y, Yan Y, Wang W and Li J 2008 *Nanotechnology* **19** 175603
[13] Yin H, Yamamoto T, Wada Y and Yanagida S 2004 *Mater. Chem. Phys.* **83** 66–70
[14] Lu L, Wang H, Xi S, Zhang H and Sun C 2008 *J. Mater. Chem.* **12** 156–8
[15] Mandal D, Bolander M E, Mukhopadhyay D, Sarkar G and Mukherjee P 2006 *Appl. Microbiol. Biotechnol.* **69** 485–92
[16] Gardea-Torresdey J L, Tiemann1 K J, Gamez G, Dokken K, Tehuacanero S and José-Yacamán M 1999 *J. Nanopart. Res.* **1** 397–404
[17] Ahmad A, Mukherjee P, Senapati S, Mandal D, Khan M I, Kumar R and Sastry M 2003 *Colloids Surf.* B **28** 313–8
[18] Sastry M, Ahmad A, Khan M I and Kumar R 2003 *Curr. Sci.* **85** 162–70
[19] Vigneshwaran N, Ashtaputre N M, Varadarajan P V, Nachane R P, Paralikar K M and Balasubramanya R H 2007 *Mater. Lett.* **61** 1413–8
[20] Yong P, Rowson N A, Farr J P G, Harris I R and Macaskie L E 2002 *Biotechnol. Bioeng.* **80** 369–79
[21] Gardea-Torresdey J L, Parsons J G, Gomez E, Peralta-Videa J, Troiani H E, Santiago P and Yacaman M J 2002 *Nano Lett.* **2** 397–401
[22] Huang J *et al* 2007 *Nanotechnology* **18** 105104
[23] Shankar S S, Ahmad A, Pasricha R and Sastry M 2003 *J. Mater. Chem.* **13** 1822–6
[24] Shankar S S, Rai A, Ahmad A and Sastry M 2005 *Chem. Mater.* **17** 566–72
[25] Zhou T, Fan G, Hong Z, Chai Y and Wu Y 2005 *J. Chromatogr.* A **1100** 76–8

[26] Zhang B, Yang R, Zhao Y and Liu C Z 2008 *J. Chromatogr.* B **867** 253–8
[27] Chen Y, Zhang H, Tian X, Zhao C, Cai L, Liu Y, Jia L, Yin H X and Chen C 2008 *Food Chem.* **109** 484–92
[28] Xiang Z and Ning Z 2008 *LWT—Food Sci. Technol.* **41** 1189–203
[29] Koo H J, Lim K H, Jung H J and Park E H 2006 *J. Ethnopharmacol.* **103** 496–500
[30] Nemamcha A, Rehspringer J L and Khatmi D 2006 *J. Phys. Chem.* B **110** 383–7
[31] Teranishi T and Miyake M 1998 *Chem. Mater.* **10** 594–600
[32] Wang Z, Shen B and He N 2004 *Mater. Lett.* **58** 3652–5
[33] Sun Y, Zhang L, Zhou H, Zhu Y, Sutter E, Ji Y, Rafailovich M H and Sokolov J C 2007 *Chem. Mater.* **19** 2065–70
[34] Rai A, Singh A, Ahmad A and Sastry M 2006 *Langmuir* **22** 736–41
[35] Takasaki M, Motoyama Y, Higashi K, Yoon S, Mochida I and Nagashima H 2007 *Chem. Asian J.* **2** 1524–33
[36] Zhao C, Wang H, Yan N, Xiao C, Mu X, Dyson P J and Kou Y 2007 *J. Catal.* **250** 33–40